5094 *Macromolecules* **2010**, *43*, 5094–5102
DOI: 10.1021/ma1004869

Macromolecules
ARTICLE

Dynamics of Natural Rubber as a Function of Frequency, Temperature, and Pressure. A Dielectric Spectroscopy Investigation

P. Ortiz-Serna,*,† R. Díaz-Calleja,† M. J. Sanchis,† G. Floudas,‡ R. C. Nunes,§ A. F. Martins,§ and L. L. Visconte§

†*Departamento de Termodinámica Aplicada, E.T.S.I.I., Instituto de Tecnología Eléctrica, Universidad Politécnica de Valencia, Camino de Vera s/n, 46022 Valencia, Spain,* ‡*Department of Physics, University of Ioannina, 451 10 Ioannina, Greece, and Foundation for Research and Technology-Hellas (FORTH), Biomedical Research Institute (BRI), and* §*Instituto de Macromoleculas Professora Eloisa Mano, Universidade Federal do Rio de Janeiro, P.O. Box 68525, Brazil*

Received March 4, 2010; Revised Manuscript Received April 30, 2010

ABSTRACT: Natural rubber (NR) isolated from *Hevea Brasiliensis* was investigated by differential scanning calorimetry, dielectric spectroscopy, and high-pressure dielectric spectroscopy. In the range of frequencies (5×10^{-2} to 3×10^{6} Hz), temperatures (−120 to 120 °C), and pressures (0.1 to 240 MPa) studied, the dielectric spectra exhibit two overlapped α-processes but no subglass relaxations. Thermal measurements revealed the presence of some moisture in NR. To elucidate the influence of water, dielectric measurements were carried out in dry and wet NR samples. The origin of the two dielectrically active processes was discussed in terms of (i) the apparent activation volume, (ii) the pressure coefficient of the respective glass temperatures, and (iii) the values of the ratio of activation energies, at constant volume and pressure. The latter allowed extracting the relative contribution of thermal energy and volume for each dynamic process. On the basis of these results, the faster α-processes is assigned to the rigidified rubber backbone dynamics whereas the slower to fatty acids (such as stearic acid) that are linked to the rubber chain.

1. Introduction

Natural rubber (NR) is a native product extracted from tropical trees of the species of *Hevea Brasiliensis* for use purposes many years before the popularization of Goodyear's elastomeric rubber. NR is well-known for its good electrical resistance and hence its potential use as an insulating material.[1,2]

The primary production of NR Latex is the cultivation of *Hevea Brasiliensis* trees and tapping of latex. Samples studied in this work come from Brazil where NR is a very abundant natural resource. This NR isolated from *Hevea Brasiliensis* is a multicomponent system containing a rubber hydrocarbon and certain proteins and lipids. Specifically, there are two types of long chain fatty acids present in NR: fatty acids linked to rubber chain at the chain-terminal and those present as a mixture. Kawahara et al.[3] found that the composition of linked fatty acids is similar to that of mixed acids; i.e., the major components are stearic acid, linoleic acid, and linoleinic acid. The reported composition of the linked and mixed stearic acid in a commercial NR was 1.05 and 4.53 mmol/kg, respectively. The mixed fatty acids are expected to link to the rubber as phospholipids.

It is well-known that changing the local structure of a polymer chain, for example by specific interactions such as hydrogen bonding, can affect significantly the local segmental dynamics.[4] However, little is known on how the segmental dynamics of NR are altered by the presence of fatty acids.

There exist some investigations of the mechanical and dielectric properties of rubbers and their vulcanized products.[5,6] NR consists basically of *cis*-poly(isoprene) (PI) chains that is essentially a low-polarity polymer. However, despite the low polarity, some polymers, such as PI, have asymmetry in their repeat unit. Because of this lack of symmetry, *cis*-PI possess nonzero components of the dipole moment both parallel and perpendicular to the chain contour.[7,8] The perpendicular component of the dipole causes a dielectric relaxation due to segmental motions, as is usually observed for polar amorphous polymers, while the parallel component give rise to a spectrum of normal modes.[9−13] At present, however, there are few reports on the dielectric relaxation of NR. In this respect, Bakule and Stoll[14] reported the occurrence of two loss maxima for a bulk NR. They considered that the low-frequency peak originates from either the parallel dipole moment of cis-PI or impurities such as proteins included in the sample. Although they did not provide a detailed analysis, the reported dielectric strength for the low-frequency process was higher than the one expected from the normal mode process.[10,11] Therefore, this low-frequency process could be associated with an impurity in their sample.

Dielectric spectroscopy (DS) is by far the more versatile technique in studying polymer and small molecule dynamics.[15−18] Although frequency and temperature are the prime variables employed by DS, pressure has emerged as the decisive thermodynamic variable on discussing the origin of the dynamic processes in polymers as well as in glass-forming liquids.[19−21] In the present study, in an effort to explore in detail the origin of the complex dynamics in NR, we employ both temperature- and pressure-dependent DS. This allows extracting all relevant thermodynamic and dynamic properties of the two processes that help identifying their origin. On the basis of the present investigation, the faster α-processes is assigned to the rigidified rubber backbone dynamics whereas the slower to fatty acids (such as stearic acid) that are linked to the rubber chain.

2. Experimental Section

Sample. Natural rubber latex was obtained from Inducompre-Ind. Com. Prest. de Serviços Ltda. (Salvador, Brazil).

*Corresponding author. E-mail: portiz@ter.upv.es.

 Published on Web 05/13/2010

Vulcanization additives used in the rubber formulation such as stearic acid (0.5 phr), zinc oxide (6 phr), sulfur (3.5 phr), *N*-*tert*-butylbenzothiazole-2-sulfenamide (TBBS) (0.7 phr), and 4,4′-dioctyldiphenylamine (1 phr) are present in the sample. The material was processed to obtain sheets with thickness of about 0.2 mm.

Nuclear Magnetic Resonance Spectroscopy (NMR). Solid-state ^{13}C NMR measurements were performed in a Bruker Avance 400 spectrometer equipped with a 89 mm wide bore, 9.4 T superconducting magnet (^{1}H and ^{13}C Larmor frequencies at 400.14 and 100.61 MHz, respectively). The data were acquired at a temperature of 295 K, with a standard Bruker double-resonance 4 mm cross-polarization (CP)/magic angle spinning (MAS) NMR probe head using 90° ^{1}H and ^{13}C pulse lengths between 3.1 and 4.5 μs. The MAS spinning rate was 6.0 kHz. The rubber sample was cut in small pieces and packed in a 4 mm zirconia rotor and sealed with Kel-F cap. The ^{13}C CP/MAS NMR spectrum was obtained by averaging 7000 scans with high-power proton decoupling (57 kHz), contact time of 5 ms, and repetition rate of 3 s. The free induction decay (FID) was processed using the spectrometer manufacturer's software. The spectrum was externally referenced to adamantane, secondary to TMS.

Differential Scanning Calorimetry (DSC). DSC[22,23] thermograms were made in the as received sample and also in a second heating ramp to reduce the possible water content. Calorimetric glass transition temperature (T_g), measured at 10 °C/min in the first and second heating ramp, was obtained in DSC-Q10 from TA Instruments. The gas used in the DSC-Q10 to obtain an inert atmosphere was N_2.

Dielectric Spectroscopy (DS). DS was performed on a Novocontrol broadband dielectric spectrometer system, based on an Alpha analyzer and a Quatro temperature controller. NR isothermal measurements were carried out at 44 frequencies between 5×10^{-2} and 3×10^{6} Hz and from −120 to 120 °C in 5 °C intervals on disk-shaped films of about 0.2 mm thickness and 20 mm diameter.

Pressure-Dependent Dielectric Spectroscopy. High-pressure dielectric spectroscopy (HPDS) was performed on a Novocontrol BDS system composed of a Solartron Schlumberger FRA 1260 frequency response analyzer and a broadband dielectric converter for frequencies in the range from 10^{-2} to 10^{6} Hz. The disk-shaped film of about 0.2 mm thickness was placed between two parallel electrodes with 20 mm diameter. The measurements under hydrostatic pressure were carried out in a Novocontrol pressure cell. The pressure setup consisted of a temperature controlled cell, hydraulic closing press with air pump, and air pump for hydrostatic test pressure. The sample cell was isolated with a Teflon ring from the surrounding silicone oil that was the pressure transmitting liquid. Isothermal measurements were carried out at several frequencies between 2×10^{-2} and 9×10^{5} Hz and several pressures between 0.1 and 240 MPa from −5 to 40 °C in 5 °C intervals. The isothermal frequency sweeps were made with temperature stability better than ±0.1 °C and pressure stability better than ±2 MPa.

3. Results and Discussion

Sample Characterization. The ^{13}C NMR spectrum is shown in Figure 1. The signal at 185.3 ppm was assigned to the acid group of the lipid present in the NR sample. Signals at 135.3 and 125.8 ppm correspond to the aromatic carbons of the vulcanization additives present in NR. Finally, the group of peaks detected between 24 and 33 ppm are assigned to the aliphatic carbons of the NR and the stearic acid.

Thermal Properties. The DSC thermograms are plotted in Figure 2. The first heating ramp exhibits a step at −60.2 °C, signifying the rubber glass temperature (T_g) and an endothermic peak at about 100 °C associated with the presence of humidity. This peak is quite broad because water evaporation takes place over a wide range of temperatures. From the heat of evaporation of bulk water (2400 J/g at 100 °C), we estimate the amount of moisture present in the sample at 0.29%. On the other hand, in the thermogram corresponding to the second heating ramp only the NR glass temperature is evident (at −60.0 °C). Clearly this value is higher than the glass temperature of bulk *cis*-PI (reported values are −78 °C (M_W = 550 000 g/mol),[9] −70 °C (M_W = 10 800 g/mol),[12] −65 (M_W = 26 000 g/mol),[13] and −72 °C (M_W = 180 000 g/mol)[24]) as a result of the mixed fatty acids that link to the rubber backbone and modify its rigidity.

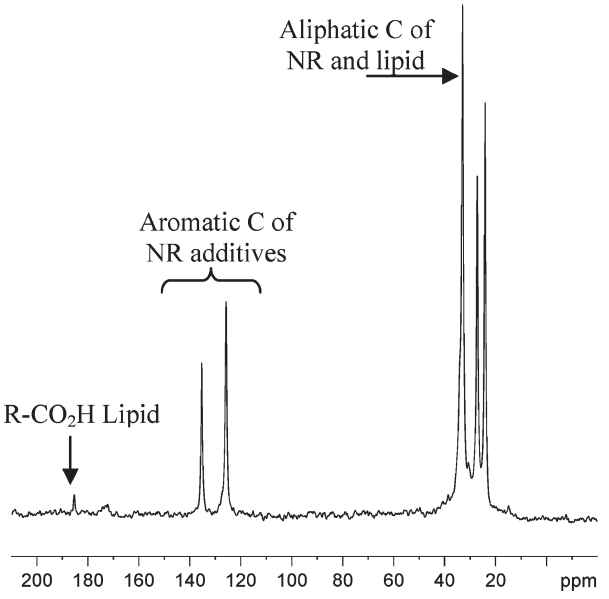

Figure 1. ^{13}C NMR spectrum for NR sample.

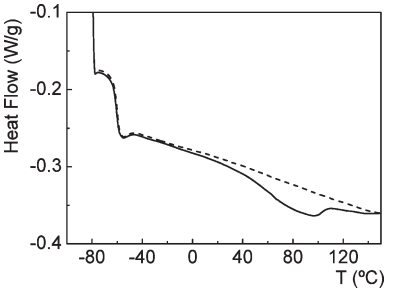

Figure 2. DSC curves taken at 10 °C/min on the first (solid line) and second heating (dashed line) of NR.

Dynamics. The thermal measurements revealed the presence of some moisture in the as-received NR sample (called "wet" below). Since NR has no hydrophilic groups, this observations suggest that water is connected to the hydroxyl groups (−OH) of the lipid component present in NR. In order to elucidate the influence of the presence of water, dielectric measurements were carried out in both "wet" and "dry" samples. The latter NR was obtained via drying in an air-circulating oven at 70 °C until constant weigh (∼1 month). Such long times and moderate temperatures were necessary to eliminate the water and to avoid the vulcanization process in the sample. We assume that there is no loss of NR components during the drying procedure because the boiling points of all them are quite above 70 °C: 361 °C for stearic acid, 2360 °C for zinc oxide, 444.7 °C for sulfur, 165 °C for TBBS, and 213 °C for 4,4′-dioctyldiphenylamine. A value of 0.28% of moisture is determined from the weight loss of the sample. This quantity agrees with the value

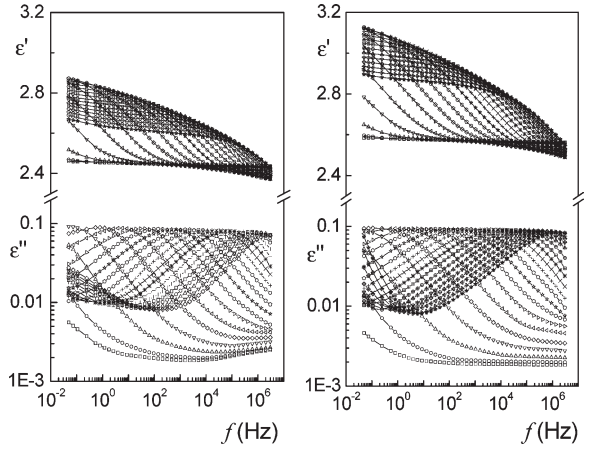

Figure 3. Dielectric permittivity (top) and loss factor (bottom) for NR from −70 to 30 °C (step 5 °C). Left: wet NR, right: dry NR (this distribution is used in all the following figures).

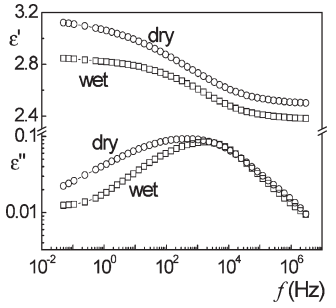

Figure 4. Comparison of wet and dry dielectric permittivity (top) and loss factor (bottom) for NR at −25 °C.

estimated by DSC, 0.29%, so we can consider that after following the above drying procedure the sample is in the water-free, i.e., dry state.

Figure 3 shows the frequency dependence of the dielectric permittivity and loss factor at different temperatures for the wet and dry NR samples. The asymmetric broadening of the dielectric loss curves is suggestive of two dynamic processes closely spaced in frequency.

The effect of removal of water from NR can best be shown by comparing, in Figure 4, the dielectric permittivity and loss spectra of the wet and dry samples at −25 °C.

It can be seen that the dielectric permittivity is higher for the dry sample and the loss curve is more asymmetric toward the low-frequency side. At first glance this is surprising. Nevertheless, similar effects have been seen in lipid membranes[25−27] that are widely analyzed because of the importance of water/lipid interactions in understanding the molecular processes in living cells. Studies with different experimental techniques revealed that dynamics of these lipids membranes cover a large range of time and length scales and depend strongly on the hydration of the membranes. In addition, the water/lipid interactions cause structural ordering in the nearest water molecules. At low temperatures, the lipid is in the *smectic-A* phase, which is structurally highly ordered. At high temperatures, the lipid hydrocarbon chains are essentially packed into a rigid and rather ordered structure, forming a *gel*. As the temperature rises, the hydrophobic region assumes a fluid disordered phase (melted hydrocarbon chains). Therefore, the lipid/water system exhibits a rich behavior as a function of temperature and water content. Moreover, in the course of dehydration, the liquid crystalline phase is able to transform into many different gel phases.[28] Dielectric permittivity is reported to be larger in the gel phase than in the liquid crystalline phase,[29,30] as experimentally observed. Thus, the higher dielectric permittivity in the dry sample likely reflects the different lipid conformation characteristic of the gel phase.

Taking into account the strong effect of water elimination from the low-frequency side of the dielectric spectra, as well as the results that will be discussed below, the slower process is assigned to the lipid dynamics. Furthermore, the temperature of the maximum at 1 Hz (−49 °C) for the slower process is in good agreement with the glass temperature of stearic acid[31] (−50 °C), which is the lipid present in NR sample as a vulcanization additive. The estimated amount of stearic acid present in NR was about 0.66 phr, of which 0.5 phr was added as a vulcanization additive and 0.16 phr is the amount calculated by Kawahara et al.[3] to be present in a commercial NR. Despite this low quantity of stearic acid, its contribution is more significant than NR because of the polar acidic groups. As described by the Onsager[32] theory, the dielectric strength relaxation is directly proportional to the square molecular dipole moment. For this and for reasons that will become clearer below we assign the slower process mainly to the lipid (labeled as α′-peak) and the faster process to the modified segmental process of NR (labeled as α-peak). As a last remark, it is clear that the slower process is not related to the spectrum of normal mode because of the network structure that suppresses the fluctuations of the chain ends.

The analysis of the dielectric spectra was made by using the empirical equation of Havriliak and Negami (HN).[33,34] In this model, the frequency dependences of the dielectric complex permittivity (ε^*) can be described by

$$\frac{\varepsilon^*(\omega)-\varepsilon_\infty}{\varepsilon_0-\varepsilon_\infty} = [1+(i+\omega\tau_0)^{\alpha}]^{-\beta} \tag{1}$$

where ε_0 is the relaxed permittivity, ε_∞ is the unrelaxed permittivity, the parameters α and β [$0<\alpha$, $\alpha\beta\le 1$] define the symmetrical and asymmetrical broadening of the loss peak, respectively, and τ_0 is the characteristic relaxation time. The relation between τ_0 and τ_{max} is given by[35]

$$\tau_{max} = \tau_0\left[\frac{\sin\dfrac{\pi\alpha\beta}{2(1+\beta)}}{\sin\dfrac{\pi\alpha}{2(1+\beta)}}\right]^{1/\alpha} \quad ; \quad f_{max} = \frac{1}{2\pi\tau_{max}} \tag{2}$$

where f_{max} is the frequency at which ε'' passes through the maximum. The splitting of eq 1 in real and imaginary parts gives

$$\varepsilon'(\omega) = \varepsilon_\infty + r^{-\beta/2}(\varepsilon_0-\varepsilon_\infty)\cos\beta\theta \tag{3}$$

$$\varepsilon''(\omega) = r^{-\beta/2}(\varepsilon_0-\varepsilon_\infty)\sin\beta\theta \tag{4}$$

where

$$r = \left[1+(\omega\tau_0)^{\alpha}\sin\left(\alpha\frac{\pi}{2}\right)\right]^2 + \left[(\omega\tau_0)^{\alpha}\cos\left(\alpha\frac{\pi}{2}\right)\right]^2$$

$$\theta = \arctan\left[\frac{(\omega\tau_0)^{\alpha}\cos\left(\alpha\dfrac{\pi}{2}\right)}{1+(\omega\tau_0)^{\alpha}\sin\left(\alpha\dfrac{\pi}{2}\right)}\right] \tag{5}$$

In the analysis of the dielectric loss spectra an additive rule for the permittivity was assumed.[36] For both wet and dry samples, the analysis of the dielectric spectra was carried out

Table 1. HN Fit Parameters for $\varepsilon''(f)$ Dependencies at Several T for α′- and α-Processes of NR

NR Measured As-Received ("Wet")

	α′-relaxation				α-relaxation			
T (°C)	$\Delta\varepsilon$	log τ (s)	α	β	$\Delta\varepsilon$	log τ (s)	α	β
−45	0.393	−0.72	0.385	1	0.133	−1.88	0.658	1
−40	0.384	−1.56	0.386	1	0.128	−2.65	0.662	1
−35	0.375	−2.30	0.389	1	0.122	−3.26	0.663	1
−30	0.367	−2.92	0.389	1	0.117	−3.83	0.672	1
−25	0.359	−3.51	0.392	1	0.111	−4.31	0.677	1
−20	0.352	−4.02	0.395	1	0.107	−4.74	0.679	1
−15	0.345	−4.48	0.400	1	0.102	−5.16	0.684	1
−10	0.339	−4.90	0.405	1	0.099	−5.53	0.687	1
−5	0.333	−5.29	0.410	1	0.095	−5.85	0.691	1
uncertainty	±0.006	±0.02	±0.002	±0.001	±0.006	±0.01	±0.007	±0.001

NR Measured in "Dry" Conditions

	α′-relaxation				α-relaxation			
T (°C)	$\Delta\varepsilon$	log τ (s)	α	β	$\Delta\varepsilon$	log τ (s)	α	β
−45	0.598	−0.21	0.350	1	0.108	−1.90	0.591	1
−40	0.589	−1.03	0.348	1	0.104	−2.63	0.599	1
−35	0.583	−1.75	0.347	1	0.098	−3.25	0.606	1
−30	0.575	−2.40	0.349	1	0.091	−3.80	0.614	1
−25	0.570	−2.96	0.346	1	0.088	−4.25	0.622	1
−20	0.563	−3.48	0.348	1	0.082	−4.68	0.629	1
−15	0.553	−3.95	0.348	1	0.080	−5.10	0.636	1
−10	0.544	−4.38	0.349	1	0.077	−5.40	0.645	1
−5	0.535	−4.78	0.350	1	0.075	−5.71	0.652	1
uncertainty	±0.005	±0.02	±0.002	±0.001	±0.004	±0.02	±0.006	±0.001

by means of the addition of two HN functions corresponding to the α and α′ processes according to

$$\frac{\varepsilon^*(\omega)-\varepsilon_\infty}{\varepsilon_0-\varepsilon_\infty}=\sum_{i=1}^{2}[1+(i\omega\tau_{0i})^{\alpha_i}]^{-\beta_i} \quad (6)$$

The frequency dependences of the loss permittivity can be evaluated by means of

$$\varepsilon''(\omega)=\sum_{i=1}^{2} r^{-\beta_i/2}(\varepsilon_0-\varepsilon_\infty)_i \sin\beta_i\theta_i \quad (7)$$

The deconvolution of ε'' was carried out by means of a multiple nonlinear regression analysis of the experimental data, allowing the eight parameters (i.e., $\Delta\varepsilon_\alpha$, α_α, β_α, τ_α, $\Delta\varepsilon_{\alpha'}$, $\alpha_{\alpha'}$, $\beta_{\alpha'}$, $\tau_{\alpha'}$) to vary. Table 1 summarizes the fit parameters, and the uncertainty in each of these parameters, obtained at several temperatures.

An example of the deconvolution procedure is depicted in Figure 5 for the α- and α′-relaxations in the dry and wet samples at −25 °C. Values of the strength of the α and α′ relaxations are summarized in Table 1 (and Figure S1 in the Supporting Information).

Briefly, the temperature dependence of the strength of the processes follows the classical trend; i.e., it decreases with increasing temperature. The strength relaxation intensity is higher for the α′-process than for the α-process, according to the larger number of dipoles present in the SA (see Figure S1 in the Supporting Information). As expected, the strength of the α-process is only slightly affected by the presence of water. However, the strength of the α′-process is strongly affected by the presence of water. This is in accordance with the notion that the α′-process is associated with the presence of the lipid (with hydrophilic groups) added to NR.

Values of the shape parameters for the deconvoluted relaxation processes, for both wet and dry NR, are summarized in Table 1 (and Figure S1 in the Supporting Information).

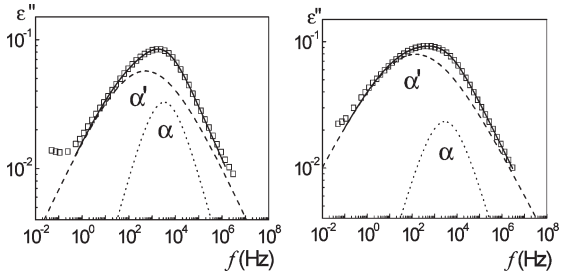

Figure 5. Deconvolution of loss factor for NR at −25 °C into two relaxation processes. Squares represent the experimental data, continuous line the HN fitting curve, and dashed lines the individual processes.

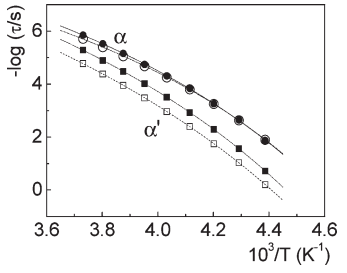

Figure 6. Arrhenius representation of the α-process (circles) and α′-process (squares) relaxation times at maximum loss for the dry (open symbols) and wet (filled symbols) NR. The dashed lines are the fits to the VFT equation.

The results with respect to the shape parameters indicate that both relaxations have distributions that are nearly temperature independent. However, the low-frequency parameter α_{HN} for the α′-process is substantially lower as compared to the α-process at all temperatures investigated (about 0.4 as compared to ∼0.7), indicating a wider distribution of relaxation times for the slower process. For both wet and dry NR samples, at all temperatures investigated, the value of β_{HN}

Table 2. VFT Fit Parameters and Relative Free Volume for α′- and α-Processes of NR

NR As-Received ("Wet")

α′-relaxation					α-relaxation				
log τ_0 (s)	D_T	T_0 (°C)	T_g (°C) at 1 s	ϕ/B	log τ_0 (s)	D_T	T_0 (°C)	T_g (°C) at 1 s	ϕ/B
−13.3 ±0.1	12.8 ±0.4	−115.1 ±1	−48.8 ±8	0.033 ±0.004	−12.5 ±0.3	10.2 ±0.7	−112.3 ±2	−55.2 ±16	0.04 ±0.01

NR "Dry"

α′-relaxation					α-relaxation				
log τ_0 (s)	D_T	T_0 (°C)	T_g (°C) at 1 s	ϕ/B	log τ_0 (s)	D_T	T_0 (°C)	T_g (°C) at 1 s	ϕ/B
−13.4 ±0.1	15.2 ±0.4	−120.9 ±0.9	−46.2 ±6	0.032 ±0.003	−11.6 ±0.2	8.5 ±0.4	−107.6 ±2	−55.3 ±12	0.037 ±0.009

was 1, and eq 1 reduces to the Cole−Cole[37] equation that describes relaxation with a symmetric distribution of relaxation times.

The relaxation times of the dry and wet NR are plotted in Figure 6 at atmospheric pressure. It can be seen that although the rate of the α-process is unaffected by eliminating water, the slower process becomes even slower in the dry sample. This can be explained by the fact that lipids contain hydrophilic acid groups ($-CO_2H$) that are solvated in the wet state. Thus, the role of water is to act as plasticizer for the lipid process, decreasing the respective glass temperature (speed-up of the dynamics).

The temperature dependence of both dynamic processes were analyzed by means of the Vogel−Fulcher−Tammann (VFT) equation[38−40]

$$\tau_{max} = \tau_0 \exp\left(\frac{D_T T_0}{T - T_0}\right) \quad (8)$$

where D_T is a dimensionless parameter and T_0 is the "ideal" glass temperature located below T_g. On the other hand, the Doolittle equation[41,42] establishes that the relaxation time associated with the α-process depends on the free volume according to

$$\tau_{max} = \tau_0 \exp\left(\frac{B}{\phi}\right) \quad (9)$$

where ϕ is the fraction of free volume. From eqs 8 and 9 it can be readily shown that

$$\frac{\phi}{B} = \frac{T - T_0}{D_T T_0} \quad (10)$$

which relates the free volume in the Doolittle equation ϕ with the values of D_T in eq 8. From the values of D_T, the relative free volume at T_g, ϕ/B, can be estimated. The values obtained for the relevant parameters of eqs 8 and 9 are shown in Table 2. The fractional free volume amounts are about 3−4% in the dry and wet NR. However, as we will see below, with respect to the pressure investigation, free volume alone cannot fully account for the dynamics. Additional information is needed on the role of thermal energy against volume, and for this reason high-pressure dielectric spectroscopy (HPDS) is a necessity.

Both the dry and wet samples were studied by HPDS over the temperature range from −5 to 40 °C in 5 °C and for pressures up to 240 MPa. Typical dielectric loss spectra are shown in Figure 7 at 5 °C for a range of pressures. These spectra reveal a bimodal distribution at all pressures

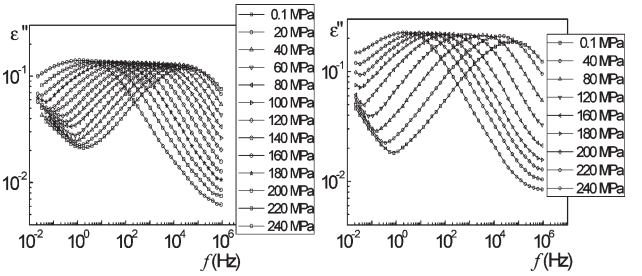

Figure 7. Loss factor for NR at 5 °C and several pressures.

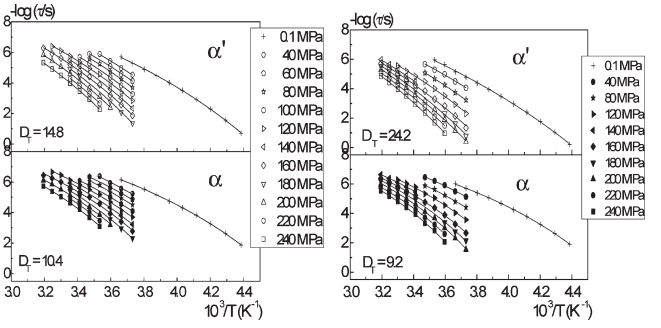

Figure 8. Isobaric relaxation times corresponding to the α′-process (top) and α-process (bottom) ε'' maximum of the NR. The lines represent the result of the fit with the temperature-VFT equation.

investigated. The Havriliak−Negami empirical model was used for the analysis of the relaxation processes, as in the T-dependent study, and the parameters for each temperature and pressure are summarized in Figures S2 and S3 of the Supporting Information.

The pressure dependence of the relaxation times corresponding to the α- and α′-processes was investigated, and the "isobaric" and "isothermal" representations for the wet and dry samples are depicted in Figures 8 and 9, respectively

$$\tau_{max} = \tau_0 \exp\left(\frac{D_P P}{P_0 - P}\right) \quad (11)$$

where D_P is dimensionless parameter and P_0 is the pressure corresponding to the "ideal" glass temperature. The corresponding D_P parameters are depicted in the two figures and show systematically lower values of D_P (and D_T) for the α-process.

Of paramount importance in polymer dynamics is the identification of the key parameters that control the segmental dynamics at temperatures near and above T_g.[43−45] According to the simplest "free" volume theory, density is

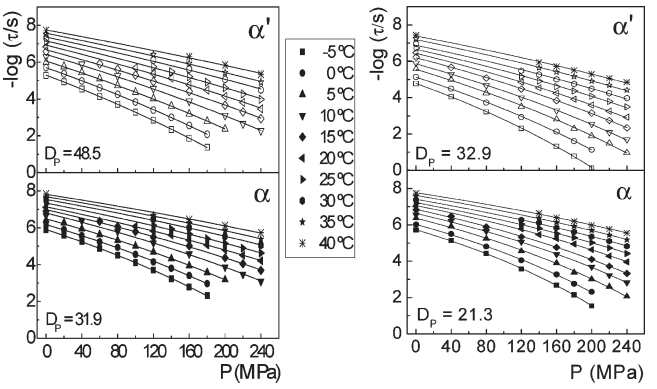

Figure 9. Isothermal relaxation times corresponding to the α′-process (top) and α-process (bottom) ε'' maximum of the NR. The lines represent the result of the fit with the pressure-VFT equation.

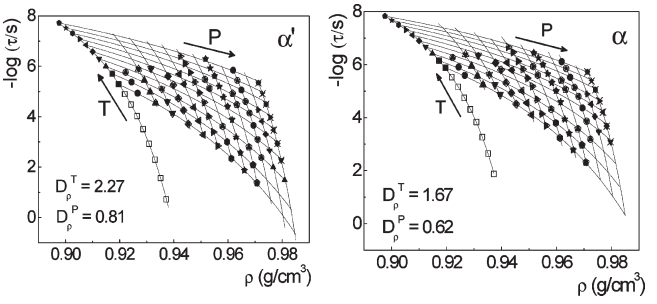

Figure 10. Dependence of the isothermal and isobaric relaxation times on density (symbols) for α′-relaxation (left) and α-relaxation (right) of the wet NR. The isothermal and isobaric lines are the results of the fits to the eq 13. The arrows indicate the increasing temperature/pressure.

the sole parameter controlling the dynamics as opposed to different "landscape" models that emphasize the importance of temperature through the associated thermal energy (k_BT). The relative contribution of density and temperature in controlling the segmental dynamics can be addressed through the density representation of the relaxation times. Standard literature data[46] of pressure−volume−temperature (PVT) for natural rubber were used for the equation of state. Subsequently, the Tait equation was employed:

$$V(P,T) = V(P_0,T)\left\{1 - 0.0894 \ln\left[1 + \frac{P}{B(T)}\right]\right\} \quad (12)$$

where $V(P_0,T) = (1.09 + 5.61 \times 10^{-4}T + 9.72 \times 10^{-7}T^2)$, with V in cm^3 g^{-1} and T in °C, is the specific volume at atmospheric pressure and $B(t) = (218.77\ \text{MPa}) \exp(-4.98 \times 10^{-3}\ T)$, with T in °C, are the parameters in the melt state.

Knowledge of the equation of state (PVT) allows casting the T- and P-dependencies of the α-relaxation times in a single representation by using the density as the only variable. In Figures 10 and 11, both the "isobaric" (at $P = 0.1$ MPa) and the "isothermal" sets of data (at 10 temperatures) are shown for the wet and dry samples, respectively. The "isothermal" relaxation times can now be described by a modified VFT equation for the density representation as[45,47]

$$\tau_{\max} = \tau_\rho \exp\left(\frac{D_\rho \rho}{\rho_0 - \rho}\right) \quad (13)$$

where D_ρ is a dimensionless parameter and ρ_0 is the density at the "ideal" glass temperature (T_0).

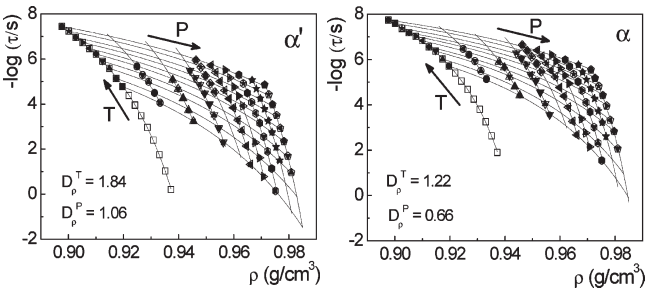

Figure 11. Dependence of the isothermal and isobaric relaxation times on density (symbols) for α′-relaxation (left) and α-relaxation (right) of the dry NR. The isothermal and isobaric lines are the results of the fits to the eq 13. The arrows indicate the increasing temperature/pressure.

A critical test of the origin of the different processes and of the relative influence of volume and temperature is provided by the value of the ratio of the apparent activation energy at constant volume, $Q_V(T,V)$, to that at constant pressure, $Q_P(T,P)$, as[48]

$$Q_V(T,V)/Q_P(T,P) = (\partial \ln \tau_\alpha/\partial(1/T)_V)/(\partial \ln \tau_\alpha/\partial(1/T)_P) \quad (14)$$

This ratio assumes values in the range 0−1 and provides a quantitative measure of the role of temperature and density on the dynamics. Values near unity suggest that the dynamics are governed mainly by the thermal energy whereas values near zero suggest that free volume ideas prevail, since in that case $Q_V = 0$. However, no polymer or glass-forming liquid has the extreme values of 0 or 1, suggesting that the picture is more complicated than the two extreme cases considered above.

In 1964, Williams[48] derived an extension of the Eyring transition state theory for chemical reactions for application to structural relaxation in polymers that gave the following equations

$$\begin{aligned} -RT^2(\partial \ln \tau/\partial T)_P &= \Delta H(T,P) + RT/2 \\ -RT^2(\partial \ln \tau/\partial T)_V &= \Delta E(T,V) + RT/2 \\ (\partial \ln \tau/\partial P)_T &= \Delta V(T,P)/RT \end{aligned} \quad (15)$$

where $\Delta H^\#$, $\Delta E^\#$, and $\Delta V^\#$ are respectively the "activation enthalpy", "activation internal energy", and "activation volume" defined with respect to unactivated and activated standard states of a relaxor. Then the ratio $Q_V(T,V)/Q_P(T,P)$ corresponds to the ratio $\Delta E^\#/\Delta H^\#$ ignoring the small term $RT/2$.

A recent study[21] provided all possibilities of extracting the dynamic ratio from dynamic and thermodynamic data. It can be readily shown that the ratio $\Delta E^\#/\Delta H^\#$ can be expressed as

$$\frac{\Delta E}{\Delta H} = 1 - \frac{\left(\dfrac{\partial \ln \tau_{\max}}{\partial \rho}\right)_T}{\left(\dfrac{\partial \ln \tau_{\max}}{\partial \rho}\right)_P} \quad (16)$$

which permits the calculation from the density representation without any extrapolations. The thus-obtained values of the ratio $\Delta E^\#/\Delta H^\#$ for the different (T, P) conditions (uncertainty for this ratio is typically 2%) are plotted in Figure 12 as a function of density. It can be seen that for the

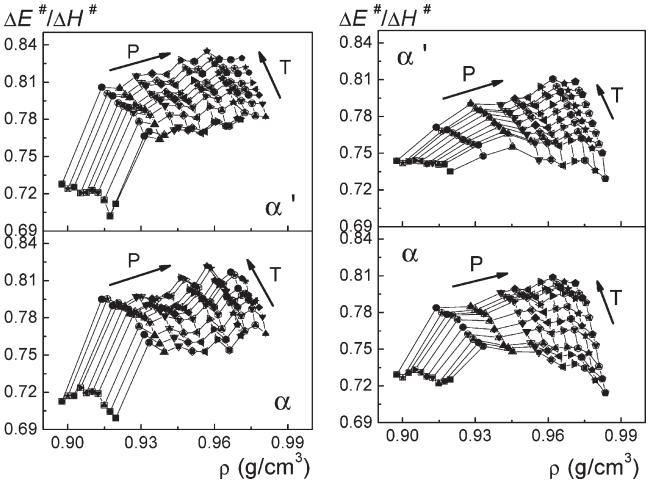

Figure 12. Ratio of the constant-volume activation energy ($\Delta E^{\#}$) to the enthalpy of activation ($\Delta H^{\#}$) plotted against density for the α′-process (top) and α-process (bottom) observed in wet (left) and dry (right) NR. The arrows indicate the increasing temperature/pressure.

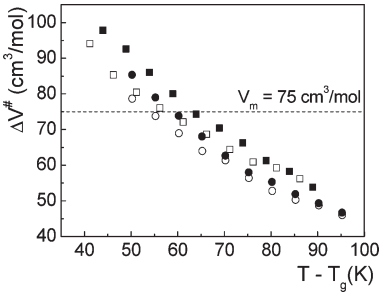

Figure 13. Apparent activation volume, $\Delta V^{\#}$, as a function of temperature for the α-process (circles) and α′-process (squares) in the dry (open symbols) and wet (filled symbols) NR. The dashed line gives the NR monomer volume.

wet NR the ratio assumes values in the range 0.70−0.82 for the α-process and values between 0.70 and 0.83 for α′-process for the different (T, P) conditions investigated. In the case of dried NR the ratio assumes again very similar values: in the range 0.71−0.81 for the α-process and between 0.73 and 0.81 for α′-process.

Recently, a correlation was demonstrated[49] between the value of the dynamic ratio at T_g and the monomeric volume. It was shown that flexible polymers with small side chains and of low monomeric volume (as the NR case) exhibit high values of the dynamic ratio, signifying the importance of temperature. Polymers with bulky side chains or large monomeric volumes exhibit lower values for the dynamic quantity, suggesting the increasing importance of density and packing on the segmental dynamics. In extreme cases of very large monomeric volumes this suggests that the free volume is the controlling parameter of the liquid-to-glass dynamics. Likewise, for the extreme case of very small monomeric volumes and flexible main-chain polymers free volume is unimportant, and the dynamics are solely controlled by the thermal energy required to explore the energy landscape. For the intermediate cases of monomeric volumes, both density and temperature are controlling the dynamics. In NR the values of the dynamic ratio being considerably above 0.5 suggest that the dynamics of both processes are affected more by temperature rather than by the available free volume. Thus, the origin of the segmental process in NR is the intramolecular barriers and the changes in local

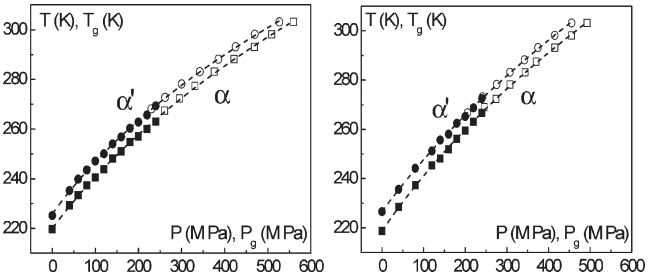

Figure 14. Pressure dependence of the glass temperatures, T_g, of the α-process (circles) and α′-process (squares) in NR. The solid symbols correspond to T_g estimated from data in isobaric and the open in isothermal conditions. Dashed lines correspond to the data fit with eq 18.

conformations brought about by the increase in temperature. In addition, the similarity in the values of the dynamic ratio for the α- and α′-processes reveals that these are intimately related.

Another measure of the effect of pressure on the dynamics can be obtained through the apparent activation volume, $\Delta V^{\#}$. This quantity can be obtained from the initial slopes of the isothermal data of Figure 9 as

$$\Delta V = RT\left(\frac{\partial \ln \tau_{\max}}{\partial P}\right)_T \tag{17}$$

originally interpreted as reflecting the difference in molar volume of activated and nonactivated species. The temperature dependence of this quantity for the α- and α′-processes in the dry and wet samples is shown in Figure 13. Notice that this quantity exhibits a strong temperature dependence on approaching T_g, and at ∼70 K above the glass temperature it becomes comparable to the monomer volume (also indicated in Figure 13).[12,13]

What is intriguing, however, is the similarity in the apparent activation volumes for the dry and wet NR samples for both processes. This again suggests the two processes are inter-related. Nevertheless, a higher apparent activation volume is found for the α′-process, which is in accord with the higher volume of relaxing species (stearic acid coupled to chain segments).

The pressure sensitivity of the glass temperatures is depicted in Figure 14 for the two processes in the wet and dry NR (T_g is operationally defined here as the temperature where the relaxation time is $\tau = 1$ s). In a PT diagram the $T_g(P)$ line can be considered as an isochronal line. The $T_g(P)$ for the two homopolymers can be described by the following empirical equation

$$T_g(P) = T_g(0)\left(1+\frac{\nu}{\mu}P\right)^{1/\nu} \tag{18}$$

first proposed by Simon and Glatzel for the melting of solid gases under pressure.[50] The same equation was subsequently employed by Andersson and Andersson[51] to describe the $T_g(P)$ of glass-forming systems. In eq 18, $T_g(0)$ is the glass temperature at atmospheric pressure and ν, μ are fitting parameters. The values of these parameters for the dry and wet NR are summarized in Table 3. It can be readily seen from Figure 14 that the initial slopes of the curves, i.e., the pressure coefficients of T_g ($dT_g/dP|_{P\to 0}$) are in the range from 0.23 to 0.25 K MPa^{-1} for the α- and α′-processes in both the wet and dry NR samples.

Thus, all measures of the segmental dynamics in NR could identify two thermally controlled and intimately related

Table 3. Parameters of eq *18* for the $T_g(P)$ Dependence

NR as-received	$T_g(0)$ (K)	μ (MPa)	ν	$dT_g/dP\|_{P\to 0}$ (K MPa^{-1})
α'-relaxation	225.9 ± 0.4	944 ± 24	3.9 ± 0.1	0.24
α-relaxation	220.0 ± 0.4	948 ± 25	3.5 ± 0.1	0.23
NR "dry"	$T_g(0)$ (K)	μ (MPa)	ν	$dT_g/dP\|_{P\to 0}$ (K MPa^{-1})
α'-relaxation	226.6 ± 0.3	986 ± 20	2.9 ± 0.1	0.23
α-relaxation	218.7 ± 0.4	884 ± 23	3.0 ± 0.1	0.25

processes. The faster process reflects the rubber backbone dynamics that is modified by the presence of stearic acid. The slower process reflects mainly the dynamics of the stearic acid that is also linked to the chain. This coupling of the fatty acid to the polymer backbone explains both the similar origin of the dynamics and the similarity in their pressure sensitivity as probed by the apparent activation volumes and the pressure sensitivities of the corresponding glass temperatures. This "dynamic structure" is in agreement with the static structure showing bonding of the fatty acids to the rubber backbone.[3,52]

4. Conclusions

The dynamics of NR, a known multicomponent system, consists of two main processes with a strong temperature and pressure dependence according to the VFT equation for temperature and pressure. The main findings of the DS study can be summarized as follows:

- The two relaxations with the strong *T*- and *P*-dependence are intimately related. The faster process reflects the rubber backbone dynamics that is modified by the presence of the stearic acid. The slower process reflects mainly the dynamics of the stearic acid that is also linked to the chain. This coupling of the stearic acid to the polymer backbone is supported by the temperature and, more importantly, the pressure DS studies.
- The dynamics of both processes are largely controlled by the thermal energy as opposed to the volume (and to free volume). This is supported by the values of the dynamic ratio being considerably above 0.5. Thus, the origin of the segmental process in NR is the intramolecular barriers and the changes in local conformations brought about by the increase in temperature. The similarity in the values of the dynamic ratio for the faster and slower processes reveals that these are intimately related.
- Although both processes have apparent activation volumes that are strongly dependent on temperature, the activation volume of the slower process is higher in accord with the assignment as reflecting the relaxation of stearic acid that is linked to the chain.
- The pressure coefficient of the glass temperature ($dT_g/dP|_{P\to 0}$) is in the range from 0.23 to 0.25 K MPa^{-1} for both processes. This shows that even at elevated pressures the two dynamic processes remain closely spaced in frequency.
- Moisture elimination from NR produce changes in the dynamics of the slower process, i.e., to the lipid dynamics, whereas the α-relaxation is not affected.
- There is no evidence for a faster process (β-process) in NR, and this is in support of the molecular interactions between the backbone and the fatty acids.

Acknowledgment. This work was financially supported by the DGCYT through Grant MAT2008-06725-C03. We also thank M[a] del Mar López and Leoncio Garrido (Instituto de Ciencia y Tecnología de Polímeros, CSIC, Madrid) for the NMR experiments.

Supporting Information Available: Figures showing *T* and *P* dependence of the HN fit parameters ($\Delta\varepsilon$ and α shape) for α'- and α-relaxation processes in wet and dry NR samples. This material is available free of charge via the Internet at http://pubs.acs.org.

References and Notes

(1) Ku, C.; Liepins, R. J. *Electrical Properties of Polymers*; Hanser Publishers: Munich, 1987.
(2) Thue, W. A. *Electrical Power Cable Engineering*; Marcel Dekker, Inc.: New York, 1998.
(3) Kawahara, S.; Kakubo, T.; Sakdapipanich, J. T. *Polymer* **2000**, *41*, 7483–7488.
(4) Ioannou, E. F.; Mountrichas, G.; Pispas, S.; Kamitsos, E. I.; Floudas, G. *Macromolecules* **2008**, *41*, 6183.
(5) Norman, R. H. *Proc. Inst. Electr. Eng.* (*London*) **1953**, *100* (IIA), 341.
(6) Scott, A. H.; McPherson, A. T.; Curtis, H. L. *J. Natl. Bur. Stand.* **1933**, *11*, 373.
(7) Stockmayer, W. H. *Pure Appl. Chem.* **1967**, *15*, 539.
(8) North, A. M. *Chem. Soc. Rev.* **1972**, *1*, 49.
(9) Adachi, K.; Kotaka, T. *Macromolecules* **1984**, *17*, 120–122.
(10) Boese, D.; Kremer, F. *Macromolecules* **1990**, *23*, 829–835.
(11) Schönhals, A. *Macromolecules* **1993**, *26*, 1309–1312.
(12) Floudas, G.; Reisinger, T. *J. Chem. Phys.* **1999**, *111*, 5201.
(13) Floudas, G.; Gravalides, C.; Reisinger, T.; Wegner, G. *J. Chem. Phys.* **1999**, *111*, 9847.
(14) Bakule, R.; Stoll, B. *Colloid Polym. Sci.* **1977**, *255*, 1176.
(15) McCrum, N. G.; Read, B. E.; Williams, W. *Anelastic and Dielectric Effects in Polymeric Solids*; Dover Publications, Inc.: New York, 1991; p 118.
(16) Kremer, F.; Schönhals, A. *Broadband Dielectric Spectroscopy*; Springer-Verlag: Berlin, 2003.
(17) Riande, E.; Díaz Calleja, R. *Electrical Properties of Polymers*; Marcel Dekker Inc.: New York, 2004.
(18) Jonscher, A. K. *Dielectric Relaxation in Solids*; Chelsea Dielectric Press: London, 1983.
(19) Floudas, G. *Prog. Polym. Sci.* **2004**, *29*, 1143.
(20) Roland, C. M.; Paluch, M.; Hensel-Bielowka, S.; Casalini, R. *Rep. Prog. Phys.* **2005**, *68*, 1405.
(21) Mpoukouvalas, K.; Floudas, G.; Williams, G. *Macromolecules* **2009**, *42*, 4690.
(22) Brown, M. E. *Introduction to Thermal Analysis. Techniques and Applications*; Kluwer Academic Publishers: Dordrecht, 2004.
(23) Balart, R.; López, J.; García, D.; Parres, F. Técnicas experimentales de análisis térmico de polímeros, Ed.ial de la Universidad Politécnica de Valencia, **2004**.
(24) Brandrup, J.; Immergut, E. H.; Grulke, E. A. *Polymer Handbook*; John Wiley & Sons Inc.: New York, 1999.
(25) Hawton, M. H.; Doane, J. W. *Biophys. J.* **1987**, *52*, 401–404.
(26) Smith, G. S.; Sirota, E. B.; Safinya, C. R.; Clark, N. A. *Phys. Rev. Lett.* **1988**, *60*, 813–816.
(27) Goldstein, R. G.; Leibler, S. *Phys. Rev. Lett.* **1988**, *61*, 2213–2216.
(28) Hung, W.-C. *WHAMPOA—Interdiscip. J.* **2007**, *52*, 47–61.
(29) Raudino, A.; Castelli, F. *J. Chem. Phys.* **2001**, *115* (17), 8238–8250.
(30) Briganti, G.; Cametti, C. *Langmuir* **2007**, *23* (14), 7518–7525.
(31) Cedeño, F. O.; Prieto, M. M.; Espina, A.; García, J. R. *Thermochim. Acta* **2001**, *369*, 39–50.
(32) Onsager, L. *J. Am. Chem. Soc.* **1936**, *58*, 1486.
(33) Havriliak, S.; Negami, S. *Polymer* **1967**, *8* (4), 161–210.
(34) Havriliak, S.; Negami, S. *J. Polym. Sci., Polym. Symp.* **1966**, *14*, 99–117.
(35) Díaz-Calleja, R. *Macromolecules* **2000**, *33*, 8924–8924.
(36) Donth, E. *J. Polym. Sci., Polym. Phys.* **1996**, *34*, 2881.
(37) Cole, K. S.; Cole, R. H. *J. Chem. Phys.* **1941**, *9*, 341.
(38) Vogel, H. *Z. Phys.* **1921**, *22*, 645–646.
(39) Fulcher, G. S. *J. Am. Ceram. Soc.* **1925**, *8*, 339–340.
(40) Tammann, G.; Hesse, W. *Z. Anorg. Allg. Chem.* **1926**, *156*, 245–247.
(41) Doolittle, A. K. *J. Appl. Phys.* **1951**, *22* (12), 1471–1975.
(42) Doolittle, A. K. *J. Appl. Phys.* **1952**, *23* (2), 236–239.
(43) Naoki, M.; Endou, H.; Matsumoto, K. *J. Phys. Chem.* **1987**, *91*, 4169.
(44) Roland, C. M.; Paluch, M.; Pakula, T.; Casalini, R. *Philos. Mag.* **2004**, *84*, 1573.

(45) Papadopoulos, P.; Peristeraki, D.; Floudas, G.; Koutalas, G.; Hadjichristidis, N. *Macromolecules* **2004**, *37*, 8116.
(46) Zoller, P.; Walsh, D. *Standard Pressure-Volume-Temperature Data for Polymers*; Technomic Publ. Co.: Lancaster, PA, 1995.
(47) Mpoukouvalas, K.; Floudas, G. *Phys. Rev. E* **2003**, *68*, 031801.
(48) Williams, G. *Trans. Faraday Soc.* **1964**, *60*, 1548.
(49) Floudas, G.; Mpoukouvalas, K.; Papadopoulos, P. *J. Chem. Phys.* **2006**, *124*, 074905.
(50) Simon, F. E.; Glatzel, G. *Z. Anorg. Allg. Chem.* **1929**, *178*, 309.
(51) Andersson, S. P.; Andersson, O. *Macromolecules* **1998**, *31*, 2999.
(52) Tanaka, Y.; Kawahara, S.; Tangpakdee, J. *KGK, Kautsch. Gummi Kunstst.* **1997**, *50*, 6.